

Experimental Characterization of the Electrical and Optical Properties of Indium Tin Oxide (ITO) Thin Films

Kaddour Benyahia¹, Arsalane Chouaib Guidoum², Abdelhamid Benhaya³, Trifa Mohamed⁴

¹Energy and Materials Laboratory, University of Tamanghasset, 11000, Tamanghasset, Algeria.

kaddour.benyahia@univ-tam.dz

²Energy and Materials Laboratory, University of Tamanghasset, 11000, Tamanghasset, Algeria.

acguidoum@unvi-tam.dz

³LEA, Department of Electronics, University of Batna 2, 05000, Batna, Algeria.

a.benhaya@univ-batna2.dz

*Corresponding author(s). kaddour.benyahia@univ-tam.dz

⁴Lecturer Professor Class A

University of Mohammed Seddik Benyahia Jijel (Algeria).

mohamed.trifa@univ-jjel.dz

ARTICLE INFO	ABSTRACT
Received: 02 Jan 2024	Indium tin oxide (ITO), a tin-doped indium oxide, has gained significant attention due to its excellent electrical conductivity and high optical transparency in the visible range. Its wide direct band gap (3.5–4.3 eV) and low resistivity make it suitable for various optoelectronic applications. In this work, thin films of ITO were prepared and characterized to study their structural, optical, and electrical properties. X-ray diffraction (XRD) revealed a polycrystalline cubic structure with a (400) preferred orientation. UV–Visible spectroscopy showed high optical transmittance (>85%) and a direct band gap of about 3.8 eV. Electrical measurements confirmed low resistivity and good carrier mobility. These results highlight the potential of ITO thin films as transparent conductive electrodes for modern devices such as solar cells and display technologies.
Revised: 01 Jul 2025	
Accepted: 10 Jul 2025	
Keywords: Indium tin oxide (ITO); thin films; structural properties; optical properties; electrical characterization; transparent conducting oxide.	

Introduction

Thanks to the emergence and continuous improvement of thin film technology, the field of materials science has undergone a remarkable transformation during the past few decades. The

invention of the semiconductor transistor marked a decisive milestone in modern technology, enabling the integration of semiconductor materials into electronic components and laying the foundations of the microelectronics revolution. Since then, the electronics industry has experienced continuous and rapid development, largely driven by the growing demand for smaller, faster, and more energy-efficient devices. This technological progress has been strongly supported by advances in materials engineering, particularly in the synthesis and optimization of functional thin films.

Among the various categories of functional materials, transparent conducting oxides (TCOs) have attracted considerable attention due to their unique combination of high electrical conductivity and excellent optical transparency in the visible region. These properties make TCOs indispensable for a wide range of optoelectronic and energy-related applications. Among them, tin-doped indium oxide ($\text{In}_2\text{O}_3:\text{Sn}$), commonly known as indium tin oxide (ITO), has emerged as the most extensively studied and utilized material because of its outstanding optoelectronic characteristics, chemical stability, and ease of integration into existing industrial processes [1–4].

ITO thin films typically exhibit low electrical resistivity (in the range of 10^{-4} – 10^{-3} $\Omega\cdot\text{cm}$) coupled with high optical transmittance exceeding 85% in the visible and near-infrared regions. These exceptional features have made ITO the material of choice for applications such as transparent electrodes in flat panel displays, plasma display panels, touch screens, organic light-emitting diodes (OLEDs), and thin-film photovoltaic devices [5–9]. Furthermore, ITO coatings are employed in architectural glazing, low-emissivity windows, and antistatic or infrared-reflective (hot mirror) surfaces, where both electrical and optical functionalities are simultaneously required.

The performance of ITO films is highly sensitive to their structural quality and stoichiometry, which are in turn influenced by several deposition parameters such as substrate type and temperature, oxygen partial pressure, target composition, film thickness, and post-deposition annealing. A wide variety of deposition methods have been explored for the fabrication of ITO layers, including magnetron sputtering, pulsed laser deposition (PLD), sol–gel processes, chemical vapor deposition (CVD), and thermal evaporation [10–13]. Each of these techniques offers specific advantages concerning film uniformity, deposition rate, compositional control, and scalability, making the choice of technique a key factor in determining film quality.

Numerous studies have reported that the structural, electrical, and optical properties of ITO thin films can be substantially enhanced through appropriate optimization of the deposition and post-treatment conditions [14–21]. In particular, post-deposition annealing plays a crucial role in improving crystallinity, reducing internal stresses, eliminating oxygen vacancies, and promoting better grain boundary connectivity. These effects collectively contribute to improved carrier mobility and higher transmittance [22–26]. Understanding and controlling such mechanisms remain essential to tailoring the functional performance of ITO-based coatings for specific applications.

However, despite its technological dominance, ITO faces certain challenges, notably the limited natural availability and rising cost of indium. This has encouraged researchers to explore alternative materials, such as aluminum-doped zinc oxide (AZO), fluorine-doped tin oxide (FTO), and hybrid multilayer structures that can either complement or substitute ITO in selected devices

[27–30]. Nevertheless, ITO continues to serve as the benchmark material among TCOs, due to its superior electrical performance, long-term stability, and compatibility with standard manufacturing processes.

In this study, we present a comprehensive investigation into the synthesis and characterization of ITO thin films prepared under controlled conditions. The main objective is to analyze the influence of deposition and post-annealing parameters on the structural, optical, and electrical properties of the films. Special attention is given to the correlation between microstructural evolution, crystallographic orientation, charge carrier concentration, and optical band gap. The ultimate goal is to identify and optimize the experimental parameters that yield high-quality ITO films suitable for advanced optoelectronic and photovoltaic applications.

I. Experimental Procedure

I.1. Objective

The main objective of this work is to characterize the electrical and optical properties of thin films based on indium tin oxide (ITO).

I.2. Substrate Preparation

The substrates used for thin film deposition were prepared by cutting soda-lime glass slides into the desired dimensions using a precision dicing saw, as illustrated in Fig.1 below.

I.3. Substrate Cleaning

Prior to deposition, the glass substrates were thoroughly cleaned using an ultrasonic cleaning process. They were successively immersed for 10 minutes each in detergent, acetone, and isopropyl alcohol baths. Between each step, the substrates were rinsed with deionized water heated to approximately 90 °C to remove residual contaminants. Finally, the substrates were dried under a stream of nitrogen gas to ensure a clean and dry surface suitable for thin film deposition.

I.4. Deposition of ITO-Based Thin Films

The ITO-based thin films were deposited using a Moorfield Minilab 60 sputtering system, as shown in Fig.2. The deposition parameters were optimized to obtain uniform and adherent films. The experimental conditions are summarized as follows:

- Base pressure: 4.1×10^{-7} mbar
- Deposition pressure: 1.34×10^{-2} mbar
- RF power: 90 W
- Deposition rate: $1.9 \text{ \AA} / \text{s}$
- Final thickness: 200 nm
- Material: ITO (purity: 99.99%).

I.5. Deposition of Metal Contacts

The metallic contacts were deposited using an **electron-beam evaporation system (Moorfield Minilab 60)**, as shown in **Fig3**. This technique allows precise control of the deposition rate and film thickness, ensuring the formation of uniform and adherent metallic layers.

The experimental conditions used for the deposition are summarized below:

- **Base pressure:** 3.2×10^{-7} mbar
- **Deposition pressure:** 1.5×10^{-6} mbar
- **Beam current:** 8.5–9.8 mA
- **Acceleration voltage:** 10 kV
- **Deposition rate:** 1 Å / s
- **Final thickness:** 200 nm
- **Evaporated material:** Silver (Ag) with a purity of 99.99%

1.6. Structural Characterization

The structural analysis of the ITO thin films was performed using an **X-ray diffractometer (Equinox 3000)**, as shown in **Fig..4**. The measurements were carried out with **Cu K α radiation** ($\lambda = 1.5418$ Å). This technique was employed to identify the crystalline phases and to determine the preferred orientation of the deposited films.

The obtained **XRD pattern**, presented in **Fig..5**, reveals a diffraction peak located around **$2\theta \approx 35^\circ$** , which corresponds to the **(400)** plane of the cubic bixbyite structure of indium oxide (In₂O₃). This indicates that the deposited ITO films exhibit a **preferred crystallographic orientation along the (400) direction**, confirming good structural quality and crystalline order.

1.7. Electrical Characterization

The sample prepared for electrical characterization consisted of an **ITO-based thin film** with a thickness of **200 nm**, deposited on a **glass substrate**. To enable current injection and voltage measurement, **four silver (Ag) contacts** with a thickness of **250 nm** were deposited at the **corners of the sample**.

This configuration allows for accurate measurement of the film's **electrical resistivity, carrier concentration, and mobility** using standard techniques such as the **four-point probe** or **Hall effect method**.

The **electrical measurements** were carried out at **room temperature** using a **Hall effect measurement system**, as illustrated in **Fig. 6**. This system allows precise determination of key electrical parameters such as **resistivity (ρ)**, **Hall mobility (μ)**, and **carrier concentration (n)**. The obtained results are summarized in **Table.1**, which provides an overview of the main electrical characteristics of the deposited ITO thin films.

The results obtained using the **Hall effect measurement system** indicate that the **ITO thin film** exhibits an **n-type semiconductor behavior**, as evidenced by the **negative value of the Hall coefficient**. The material shows a **low electrical resistivity** of **$2.56 \times 10^{-4} \Omega \cdot \text{cm}$** combined with a **high carrier concentration** of **$3.86 \times 10^{21} \text{ cm}^{-3}$** , which allows ITO to be classified as a **degenerately doped semiconductor** or **highly conductive oxide**.

These findings demonstrate that the electrical performance of the deposited ITO layers is consistent with those reported in the literature [31, 32–40]. Similarly, the measured **charge carrier mobility** values are in good agreement with previously published data [109], confirming the high crystalline quality and efficient charge transport within the films.

IV.8. Optical Characterization

IV.8. Optical Characterization

Optical measurements were performed using an **F10-RT-UV spectrophotometer**, as shown in **Fig.7** below. This instrument was used to record both **transmittance** and **reflectance** spectra of the ITO thin films over a wide spectral range.

It is worth noting that appropriate analysis of the transmittance and reflectance spectra allows the determination of several important **optical parameters**, such as the **optical band gap** and the **film thickness**. These quantities provide valuable insight into the **optical quality**, **uniformity**, and **electronic properties** of the deposited ITO layers.

I.8.1. Optical Transmission

Figure 8 presents the **transmittance spectrum** of the ITO thin films in the **wavelength range of 200–1100 nm**. In the **ultraviolet (UV) region** (200–300 nm), the transmittance is relatively low, indicating strong optical absorption exceeding **60%**. This behavior is mainly attributed to the combined absorption of both the **glass substrate** and the **ITO layer**, whose **optical band gap** lies within this spectral range, characteristic of a **semiconducting material**.

In contrast, in the **visible region**, the situation is reversed: the transmittance increases significantly, as neither the substrate nor the deposited layer exhibits strong absorption. The films thus display **high optical transparency** and **low reflectance**, typical features of well-crystallized and stoichiometrically balanced ITO layers.

The combination of **high transmittance** and **low reflectance** makes ITO an excellent candidate for use as a **transparent conductive electrode** or as an **anti-reflective coating** in **organic photovoltaic cells** and other **optoelectronic applications**.

I.8.2. Energy Gap

As mentioned above, different quantities and parameters can be deduced from the transmittance and reflectance spectra. Thus, the absorption coefficient (α) can be directly deduced from the optical transmission spectrum using the following expression:

$$\alpha = -\ln(T) / d \quad (1)$$

where d is the film thickness and T is the transmittance coefficient.

The optical band gap (E_g) of the films is determined by applying the Tauc model and the Davis and Mott model in the high absorbance region, using the expression:

$$\alpha h\nu = A(h\nu - E_g)^n \quad (2)$$

Where α is the absorption coefficient, $h\nu$ is the photon energy, E_{g} is the optical band gap, and A is a constant.

For $n = 1/2$, the experimental data provide the best linear fit in the band edge region, which corresponds to a **direct allowed electronic transition**. The **optical band gap**

(E_g) of the film can be determined from the plot of $(\alpha h\nu)^2$ as a function of $h\nu$, by extrapolating the linear portion of the curve to the energy axis (Fig.9).

The estimated optical band gap is **3.8 eV**, which falls within the range of values reported in the literature (**3.5–4.3 eV**) [108, 117–120]. This result confirms the high transparency and good crystallinity of the deposited ITO thin films, consistent with their semiconducting nature and the presence of a direct optical transition.

Conclusion

The main objective of this work was to study the **optical and electrical properties** of **ITO thin films** deposited by the **sputtering technique**. The **structural characterization** was performed using an **Equinox 3000 X-ray diffractometer**, which confirmed the presence of a diffraction peak around $2\theta \approx 35^\circ$, corresponding to the **(400)** plane of a **cubic structure**. This result indicates that the deposited ITO films exhibit a **preferred crystallographic orientation** and good structural quality.

For the **electrical characterization**, a 200 nm thick ITO-based thin film was deposited on a **glass substrate**, and **four silver contacts** of 250 nm thickness were deposited at the corners of the sample. Electrical measurements were performed at **room temperature** using both the **Hall effect system** and the **four-point probe technique** to determine the **resistivity** of the deposited layer. The obtained results indicated that ITO behaves as a **highly conductive n-type semiconductor**, exhibiting a **low resistivity** of about $2.6 \times 10^{-4} \Omega \cdot \text{cm}$ and a **high carrier concentration** close to $3.86 \times 10^{21} \text{ cm}^{-3}$.

Regarding the **optical characterization**, the **F10-RT-UV spectrophotometer** was used to record the **transmittance and reflectance spectra** of the ITO layers. In the **ultraviolet (UV) region** (200–300 nm), the transmittance was found to be low, indicating strong absorption exceeding **60%**, due to both the glass substrate and the semiconducting nature of the deposited layer, whose band gap lies within this spectral range. In contrast, in the **visible region**, the transmittance was relatively high, as neither the substrate nor the thin film exhibited significant absorption.

The analysis of the transmittance spectrum allowed the determination of the **absorption coefficient** in the fundamental absorption region. The **optical band gap** was evaluated using the **Tauc, Davis, and Mott model** in the high-absorption region, yielding an estimated value of **3.8 eV**. This value is consistent with those reported in the literature and confirms the **direct band gap nature** of the ITO films.

The combination of **high transmittance** and **low reflectance** demonstrates that ITO is an excellent material for use as a **transparent electrode** or an **anti-reflective coating** in **organic photovoltaic and optoelectronic devices**.

In conclusion, the results of the **structural, electrical, and optical** characterizations clearly indicate that the **ITO thin films** produced in this work possess the required properties for **high-performance optoelectronic applications**.

Bibliographic References

- [1] Tazerout, M., Couches minces de ZnO pour applications en optique : synthèse et étude des effets de la concentration du sol, du dopage Ce et du co-dopage Ce-Li, Thèse de Doctorat, Université A. Mira - Béjaïa, 2017–2018.
- [2] Manavizadeh, N., Boroumand, F.A., Asl-Soleimani, E., Raissi, F., Bagherzadeh, S., Khodayari, A., Rasouli, M.A., Thin Solid Films 517 (2009) 2324–2327.
- [3] Zhang, X., Wu, W., Tian, T., Man, Y., Wang, J., Materials Research Bulletin 43 (2008) 1016–1022.
- [4] El Hichou, A., Kachouane, A., Bubendorff, J.L., Addou, M., Ebothe, J., Troyon, M., Bougrine, A., Thin Solid Films 458 (2004) 263–268.
- [5] Morales, E.H., Diebold, U., Applied Physics Letters 95 (2009) 253105.
- [6] Yu, H.H., Hwang, S.-J., Tseng, M.-C., Tseng, C.-C., Optics Communications 259 (2006) 187–193.
- [7] Benoy, M.D., Mohammed, E.M., Suresh Babu, M., Binu, P.J., Pradeep, B., Brazilian Journal of Physics 39 (4) (2009) 629–632.
- [8] Hartnagel, H.L., Semiconducting Transparent Thin Films, Institute of Physics Publishing, Bristol, UK (1995). ISBN 978-0750303224.
- [9] Konry, T., Marks, R.S., Thin Solid Films 492 (2005) 313–321.
- [10] Saadeddin, I., Thèse de doctorat, Université Bordeaux I, 2007.
- [11] Giusti, G., Tian, L., Jones, I.P., Abell, J.S., Bowen, J., Thin Solid Films 518 (2009) 1140–1144.
- [12] Daoudi, K., Thèse de doctorat, Université Claude Bernard Lyon 1, 2003.
- [13] Kerkache, L., Thèse de doctorat d'État, Université Ferhat Abbas Sétif (UFAS), 2006.
- [14] Viespe, C., Nicolas, I., Sima, C., Grigoriu, C., Medianu, R., Thin Solid Films 515 (2007) 8771–8775.
- [15] Bhatti, M.T., Rana, A.M., Khan, A.F., Ansari, M.I., Pakistan Journal of Applied Sciences 2 (5) (2002) 570–573.
- [16] Lan, Y.F., Peng, W.C., Lo, Y.H., He, J.L., Organic Electronics 11 (2010) 670–676.
- [17] Kim, K.-H., Choi, K., Choi, E.-S., Hwang, J.-H., Hwang, J.-T., Journal of Ceramic Processing Research 4 (2) (2003) 96–100.
- [18] Malathy, V., Sivaranjani, S., Vidhya, V.S., Joseph Prince, J., Balasubramanian, T., Sanjeeviraja, C., Jayachandran, M., Journal of Non-Crystalline Solids 355 (2009) 1508–1516.
- [19] Liu, J., Wu, D., Zeng, S., Journal of Materials Processing Technology 209 (2009) 3943–3948.

[20] Dobrikov, G.H., Rassovska, M.M., Boiadjiev, S.I., Gesheva, K.A., Sharlandjiev, P.S., Koserkova, A.S., Electronics Conference, Sozopol, Bulgaria (2007).

[21] Simashkevich, A., Serban, D., Bruc, L., Coval, A., Fedorov, V., Bobeico, E., Usatii, Iu., Spray Deposited ITO–nSi Solar Cells with Enlarged Area, Article (2004).

[22] McDonnell, C., Milne, D., Chan, H., Rostohar, D., O'Connor, G.M., “Ultra-short pulse laser patterning of very thin indium tin oxide on glass substrates”, Optics and Lasers in Engineering 77 (2016) Part 2, DOI: 10.1016/j.optlaseng.2015.11.008.

[23] Radhakrishna, M.C., Rao, M.R., Pramāna 9 (1) (1977) 1–6.

[24] Manificier, J.-C., Szepessy, L., Bresse, J.F., Percin, N.I., Stuck, R., Materials Research Bulletin 14 (1979) 163–175.

[25] Khodorov, A., Piechowiak, M., Gomes, M.J.M., Thin Solid Films 515 (2007) 7829–7833.

[26] McDonnell, C., Milne, D., Chan, H., Rostohar, D., O'Connor, G.M., Ultra-short pulse laser patterning of very thin indium tin oxide on glass substrates, Optics and Lasers in Engineering 77 (Part 2) (2016). DOI: 10.1016/j.optlaseng.2015.11.008.

[27] Radhakrishna, M.C., Rao, M.R., Pramāna – Journal of Physics 9 (1) (1977) 1–6.

[28] Manificier, J.-C., Szepessy, L., Bresse, J.F., Percin, N.I., Stuck, R., Materials Research Bulletin 14 (1979) 163–175.

[29] Manavizadeh, N., Boroumand, F.A., Asl-Soleimani, E., Raissi, F., Bagherzadeh, S., Khodayari, A., Rasouli, M.A., Thin Solid Films 517 (2009) 2324–2327.

[30] Khodorov, A., Piechowiak, M., Gomes, M.J.M., Thin Solid Films 515 (2007) 7829–7833.

[31] Shao, L.X., Chang, K.H., Hwang, H.L., Zinc sulfide thin films deposited by RF reactive sputtering for photovoltaic applications, Applied Surface Science 212–213 (2003) 305–310.

[32] Darenfed, O., Aida, M.S., Hafdallah, A., et al., Substrate temperature influence on ZnS thin films prepared by ultrasonic spray, Thin Solid Films 518 (2009) 1082–1086.

[33] Lekiket, H., Aida, M.S., Chemical bath deposition of nanocrystalline ZnS thin films: influence of pH on the reaction solution, Materials Science in Semiconductor Processing 16 (2013) 1753–1758.

[34] Subbaiah, Y.P.V., Prathap, P., Reddy, K.T.R., Structural, electrical and optical properties of ZnS films deposited by close-spaced evaporation, Applied Surface Science 253 (2006) 2409–2415.

[35] Nasir, E.M., Surface morphological and structural properties of ZnS and ZnS:Al thin films, International Journal of Innovative Research in Science, Engineering and Technology 3 (2014) 8114–8119.

[36] Urakawa, Y., Gleason, K.K., Tunable photoluminescence via thermally evaporated ZnS ultrathin films, Journal of Coating Science and Technology 1 (2014) 46–52.

[37] Yuvaraj, D., Sathyanarayanan, M., Rao, K.N., Growth of ZnS nanostructures in high vacuum by thermal evaporation, *Journal of Nanoscience and Nanotechnology* 13 (2013) 1–7.

[38] Xue, S., Effects of thermal annealing on the optical properties of Ar ion irradiated ZnS films, *Ceramics International* 39 (2013) 6577–6582.

[39] Jin, C., Kim, H., Baek, K., et al., Effects of coating and thermal annealing on the photoluminescence properties of ZnS/ZnO one-dimensional radial heterostructures, *Materials Science and Engineering: B* 170 (2010) 143–148.

[40] Li, B.H., Zhao, D.X., Yao, B., et al., The growth of single cubic phase ZnS thin films on silica glass by plasma-assisted metalorganic chemical vapor deposition, *Thin Solid Films* 513 (2006) 114–118.

Figures

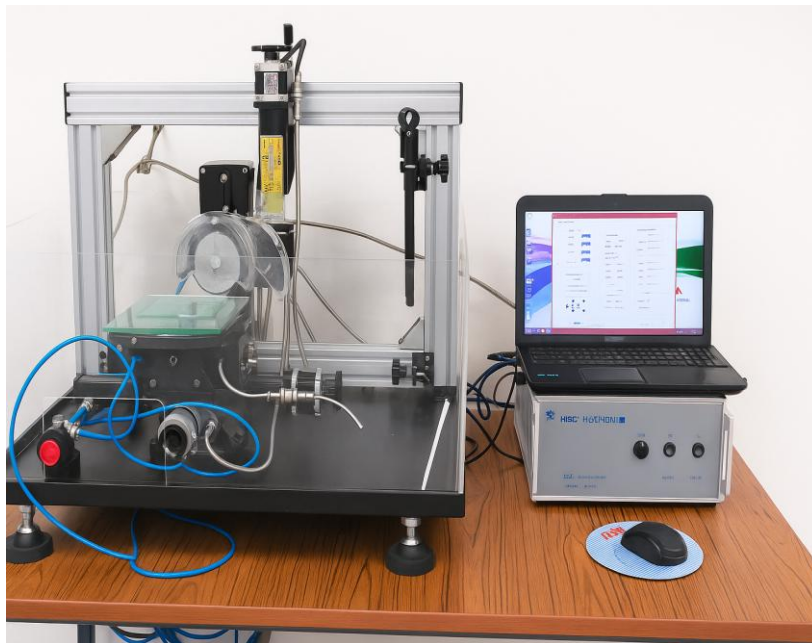


Fig.1: The dicing-cutting saw used to prepare the substrates.



Fig.2: The sputter system used to deposit ITO-based thin films.

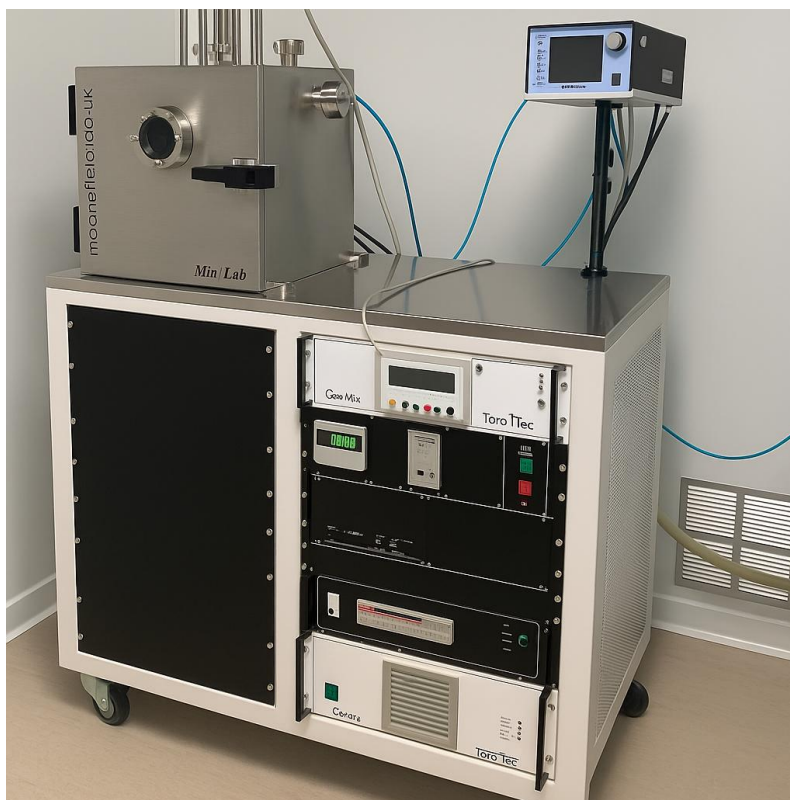


Fig.3: The e-beam system used to deposit metallic contacts.



Fig..4: Schematic illustration of equinox 3000 diffractometer.

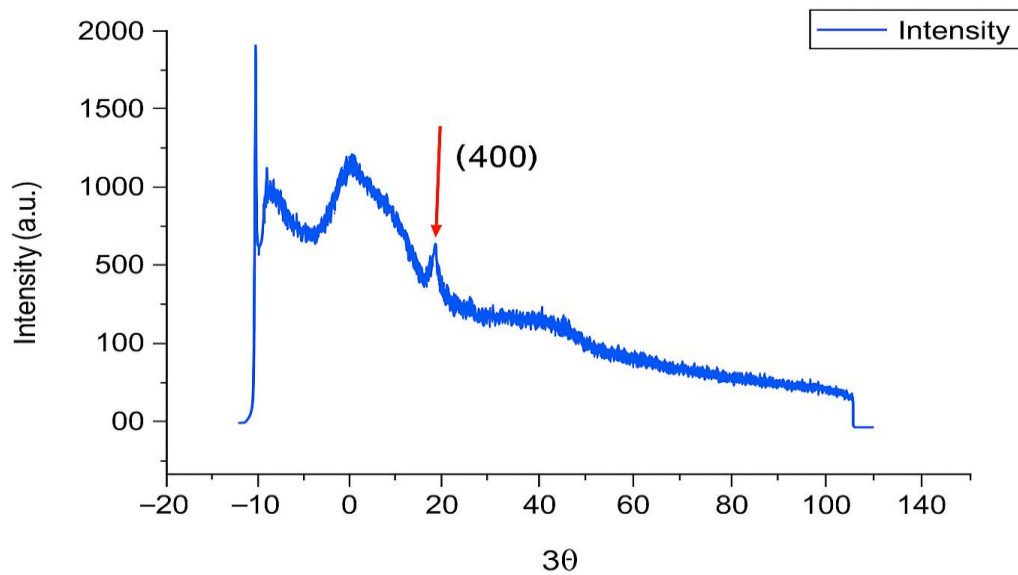


Fig..5: XRD spectra of ITO thin film.

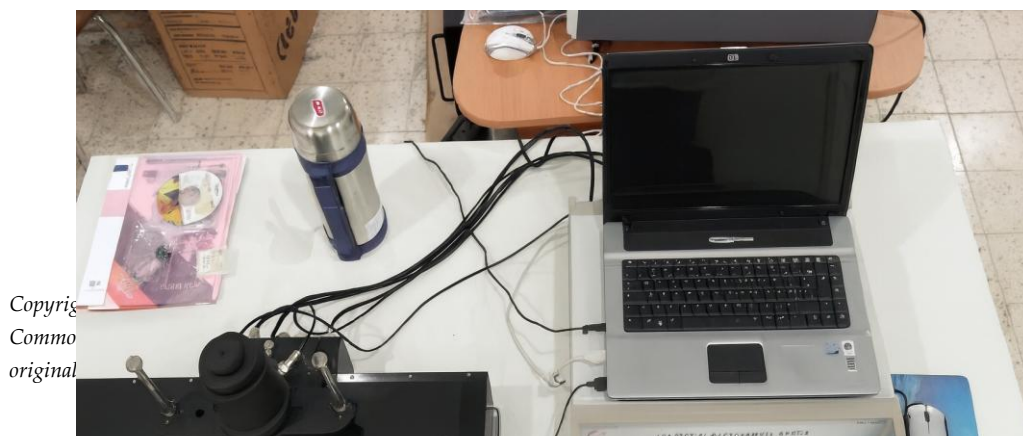


Fig.6: Hall effect system.



Fig.7: The F10-RT-UV spectrophotometer.



Fig.8: The transmittance spectrum of ITO thin films.

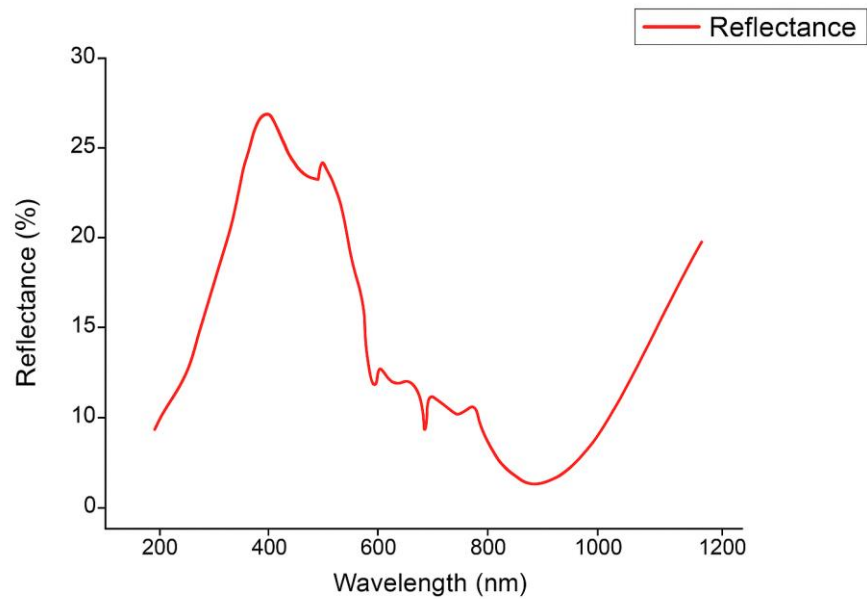


Fig.9: The reflectance spectrum of ITO thin films.

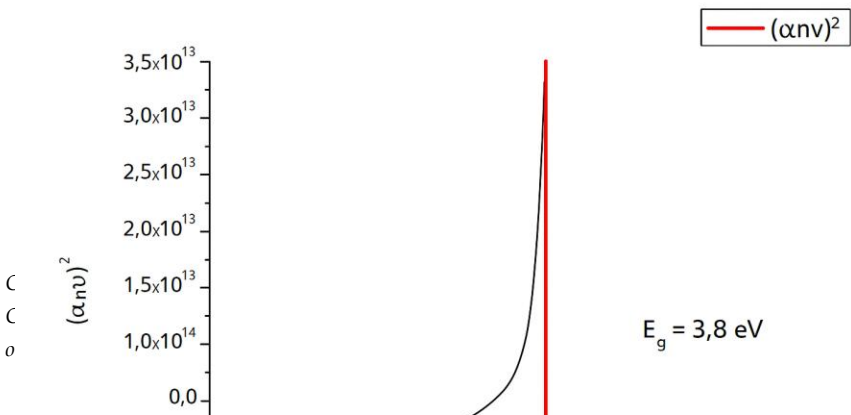


Fig.10: Variation of $(\alpha h\nu)^2$ as a function of photons energy.

Tableaux

N	T (K)	I (A)	P ($\Omega \cdot \text{cm}$)	μ ($\text{cm}^2 \text{V}^{-1} \text{s}^{-1}$)	Bulk Con. (cm^{-3})	Avg. Hall ($\text{C}^{-1} \text{cm}^3$)
1	297	1.0000E-03	2.5618E-04	6.3119E+00	- 3.8604E+21	-1.6170E-03
2	297	2.0000E-03	2.5618E-04	6.6045E+00	- 3.6893E+21	-1.6920E-03
3	297	3.0000E-03	2.5643E-04	6.9275E+00	- 3.5139E+21	-1.7765E-03
4	297	4.0000E-03	2.5641E-04	6.7650E+00	- 3.5986E+21	-1.7346E-03
5	297	5.0000E-03	2.5668E-04	6.6966E+00	- 3.6315E+21	-1.7189E-03
6	297	6.0000E-03	2.5666E-04	6.7508E+00	- 3.6027E+21	-1.7320E-03
7	297	7.0000E-03	2.5663E-04	6.7336E+00	- 3.6123E+21	-1.7280E-03
8	297	8.0000E-03	2.5664E-04	6.6669E+00	- 3.6483E+21	-1.7110E-03
9	297	9.0000E-03	2.5666E-04	6.6653E+00	- 3.6385E+21	-1.7156E-03
10	297	1.0000E-02	2.5660E-04	6.7717E+00	- 3.5924E+21	-1.7376E-03

Tab..1: Electrical measurements obtained with Hall Effect system

N°	T (K)	ρ (Ω)	Vmes aux bornes Rstand (mV)	Vmes (mV)	Range I (μA)
01	297	28.51	99.00	415.2	1
02	297	20.36	99.11	269.9	1

03	297	19.85	99.08	289.1V	1
04	297	19.88	99.01V	289.6	1

Tab..2: Electrical measurements obtained with four-point probe.